aerospace

MDPI

Article

Mission Performance Analysis of Hybrid-Electric Regional Aircraft

Giuseppe Palaia * and Karim Abu Salem

Department of Civil and Industrial Engineering, University of Pisa, Via Caruso 8, 56122 Pisa, Italy
* Correspondence: giuseppe.palaia@phd.unipi.it

Abstract: This article discusses the mission performance of regional aircraft with hybrid-electric propulsion. The performance analyses are provided by mission simulations tools specifically developed for hybrid-electric aircraft flight dynamics. The hybrid-electric aircraft mission performance is assessed for the design point, identified by top level requirements, and for off-design missions, within the whole operating envelope. This work highlights that the operating features of hybrid-electric aircraft differ from those of aircraft of the same category with conventional thermal propulsion. This assessment is processed by properly analysing the aircraft payload–range diagram, which is a very effective tool to assess the operating performance. The payload–range diagram shape of hybrid-electric aircraft can vary as multiple combinations of the masses of batteries, fuel and payload to be transported on board are possible. The trade-off in the power supply strategies of the two power sources to reduce fuel consumption or to extend the maximum flight distance is described in detail. The results show that the hybrid-electric propulsion integrated on regional aircraft can lead to benefits in terms of environmental performance, through savings in direct fuel consumption, or alternatively in operating terms, through a significant extension of the operating envelope.

Keywords: hybrid-electric aircraft; mission simulation; aircraft design; performance analysis

Citation: Palaia, G.; Abu Salem, K. Mission Performance Analysis of Hybrid-Electric Regional Aircraft. *Aerospace* **2023**, *10*, 246. https://doi.org/10.3390/aerospace10030246

Academic Editor: Sergey Leonov

Received: 24 January 2023
Revised: 17 February 2023
Accepted: 28 February 2023
Published: 2 March 2023

1. Introduction

The environmental impact of transport aircraft operations is assuming increasingly significant proportions [1]. Specifically, the significance of transport aviation in terms of climate-changing emissions in the coming years is more and more of concern. For this reason, aeronautical research is projected towards solutions to reduce the environmental impact of aviation [1–3], in agreement with the requirements imposed by authorities. For example, the European Commission aims to achieve climate neutral aviation by 2050; furthermore, an intermediate requirement is set for 2030, whereby a 55% reduction in greenhouse gas emissions must be reached [4]. Specifically, great effort is made on innovative solutions aiming at reducing aircraft emissions, both from the airframe side [5–10] and propulsion side [11–15]. In particular, hybrid-electric propulsion is currently under intense investigation as an effective solution to reduce direct emissions of transport aviation [16–18]; this work focuses on this type of propulsion.

Technological limitations related to electrical energy storage systems, which exhibit very low gravimetric energy densities compared to kerosene, make the development of medium- and long-range hybrid-electric aircraft very implausible, even considering the most optimistic future outlook for the improvement of batteries' performance. Consequently, the most interesting results have been currently achieved on the integration of electric or hybrid-electric on small aircraft, typically used for general aviation [19–21] or in the commuter sector [22–27]; efforts are also currently being made to conceive new models of electric urban air transport [28–31]. However, most of the interest in reducing the environmental impact of aircraft lies in larger transport vehicles, that contribute more to the share of greenhouse gas emissions [32]. Although several studies have focused on

the potential of electrification of short–medium-range aircraft [33–37], it appears that this category is unlikely to be considered for the integration of electric power in the coming years. For this reason, the present paper focuses on the regional aircraft category, which seems the best candidate for the earliest introduction of electrification of propulsion systems among all the commercial transport aircraft. Some relevant studies regarding this class of aircraft are described in [38–42]. Most of these works focus on the design methods and the conceptual development of hybrid-electric aircraft. Other studies, such as [43–47], focus more on technological aspects related to the development of electric machines and the on-board integration of electric power systems. Another relevant aspect for characterising the potential of hybrid-electric aircraft, on the other hand, is its comprehensive performance analysis. This paper, therefore, starting from a conceptual design task, describes a performance characterisation of a regional hybrid-electric aircraft within its entire operational envelope. The approach here represents a marked development compared to more simplified methods such as those proposed in [48,49], allowing time-dependent variables to be handled within the design loop and to be used for detailed performance analyses, or to set up optimisation processes that handle constraints such as weight and power supply. The performance analysis is carried out by adopting mission simulation techniques; specifically, the equations of motion of the aircraft, handled as a point mass, are time-integrated to evaluate aerodynamic, aeromechanical and weight characteristics at each instant of the flight, and thus to fully characterise the mission performance. The developed simulation framework is able to handle the main feature of hybrid-electric aircraft, i.e., the capability to simultaneously supply both electric and thermal power in different proportions, and to exploit the energy provided by the batteries and/or fuel combustion at each instant of the mission. Different power and energy supply strategies consequently allow the hybrid-electric aircraft to show different performance under the same initial conditions. For example, power supply strategies can be identified to minimise fuel consumption for a specific mission; alternatively, power management profiles can be set to extend the nominal range of the aircraft at the expense of higher fuel consumption. To assess these instances, a very effective tool for analysing operational performance, the payload–range diagram, has been adopted; this allowed us to outline the main operating performance differences between thermal and hybrid-electric regional aircraft.

The paper Is organised as follows: Section 2 provides the detailed design and performance analysis framework developed in this research; specifically, the reference hybrid-electric aircraft is presented, the design methodology is described and a deep focus on the mission simulation techniques is provided. Section 3 gives the results of the performance analysis in the typical design envelope of the reference hybrid-electric aircraft. Section 4 widely focuses on the whole payload–range envelope construction for the hybrid-electric aircraft. Finally, conclusions are provided in Section 5.

2. Hybrid-Electric Aircraft Design

2.1. Hybrid-Electric Aircraft Requirements

As previously mentioned, the regional category is the one that seems to be realistically the first among the transport aircraft to integrate hybrid-electric propulsion. In this work, therefore, this market sector was considered as a benchmark, and design requirements similar to those of the aircraft ATR 42 have been considered (Table 1). An interesting reference analysing the future scenario of the regional air transport sector, together with a thorough discussion of its relevant design requirements, can be found in [50].

Table 1. Regional aircraft selected TLARs.

TLARs	
Number of seats	40
Cruise Mach	0.4
Cruise altitude	20,000 ft
Design mission range	600 nm
Balanced field length	1100 m
Landing distance available	1100 m

In this work, a hybrid-electric regional aircraft capable of transporting 40 passengers over a design distance of 600 nm was designed and analysed. An artistic representation of such an aircraft, equipped with turboprop engines, is shown in Figure 1.

Figure 1. Artistic representation of a reference regional aircraft.

2.2. Conceptual Design Methodology

The design and performance analysis of hybrid-electric aircraft carried out in this work were performed using the in-house developed software THEA-CODE [51,52]. This design framework combines the classical elements of conceptual aircraft design, such as aerodynamic, structural and flight mechanics assessments, with the novel features of hybrid-electric propulsion system integration. The main modules of the design workflow, schematically sketched in Figure 2, are *Aerodynamics*, *Engine sizing*, *Mission analysis* and *Weight estimation*.

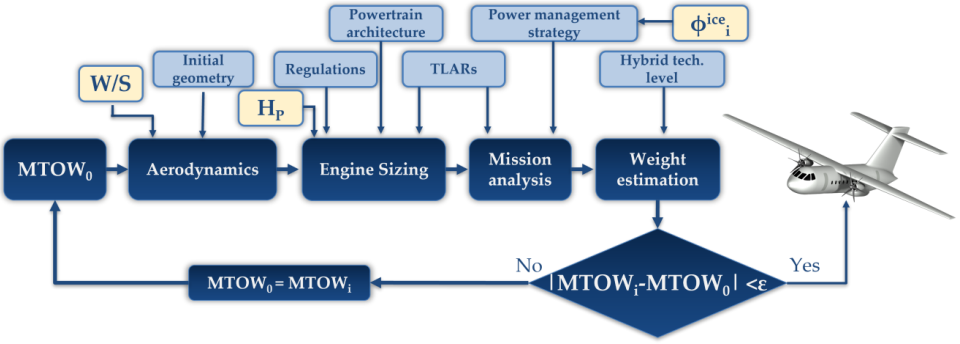

Figure 2. THEA-CODE workflow.

The *Aerodynamics* module computes the aircraft polar drag; induced drag is estimated by means of AVL [53], a vortex lattice method solver, whereas the parasitic drag of all the aircraft components is evaluated through the component build-up method [54]. The *Engine sizing* module estimates the required installed power of the hybrid-electric powertrain by means of the so-called matching chart [55,56]. Specifically, this diagram relates the aircraft specific power (P/W) with the wing loading (W/S), on the basis of the current regulations [57]. By properly handling this chart, it is possible to estimate the total power to be installed on board and how it is split between the electric motors (P^{emot}_{inst}) and the thermal engines (P^{ice}_{inst}). The degree of hybridisation H_P, i.e., the ratio between the electric motor installed power and the total installed power, is the design parameter which defines this split of installed power, and it is defined according to Equation (1).

$$H_P = \frac{P^{emot}_{inst}}{P^{emot}_{inst} + P^{ice}_{inst}} \quad (1)$$

The *Mission analysis* block simulates the aircraft flight trajectory by means of a time-marching simulation, as described in detail in Section 2.3. One of the main outputs provided by the *Mission analysis* block is the weight of the fuel and the battery required to accomplish the considered mission. The propulsion system weight is evaluated by the *Engine sizing* block as the ratio between the installed power and its specific power, for both thermal en-

gines and electric motors. The weight of the other items is evaluated in the *Weight estimation* block; specifically, operating item and system weight is computed by means of literature models [58]. Regarding the structures, lifting system weight was estimated by a FEM-based surrogate model [59]. The weight of fuselage, landing gear and vertical/horizontal tail was evaluated using the model provided in [58].

The design procedure ends if the convergence on MTOW is achieved. A constraint to be satisfied is imposed on the available internal volumes to store fuel and batteries; a qualitative scheme of possible volume allocation is depicted in Figure 3.

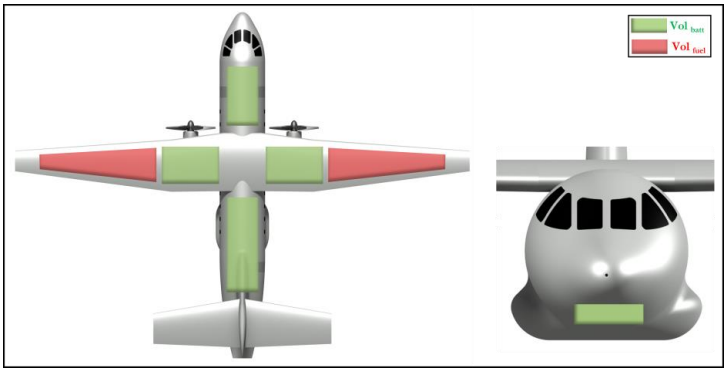

Figure 3. Qualitative scheme of fuel and battery available volume distribution.

The electric powertrain component main performances used as references in this context are: battery energy density (BED) at pack level = 500 Wh/kg, and electric motor power density = 15 kW/kg [60]. A residual 20% of battery state of charge (SoC) is imposed at the end of the mission.

2.3. Mission Simulation and Performance Analysis

2.3.1. Overview

Performance analysis is a crucial aspect in the design and development process of an aircraft. As aeroplanes are complex machines, there are many different figures of merit that can characterise their performance [61]. In the case of commercial aircraft, figures of merit related to costs, pollutant emissions, fuel consumption, maximum take-off weight, etc., have a fundamental importance in steering the design choices, from the early stages of the conceptual design. The study of aircraft performance allows us to correlate its general features, such as aerodynamic, propulsive and weight characteristics, with the typical outputs of a flight mission, such as distance flown, flight time, fuel consumption, etc. In order to carry out such performance studies, it is necessary to provide an effective mathematical model of the aircraft and the external environment, specific to the conditions to be assessed. Starting from the complete equations of motion of the aircraft, and gradually introducing a series of proper simplifications, it is possible to derive the dedicated model for the performance analysis carried out in this study. The simplified model followed in this work, briefly outlined below, is taken from [62]. The first main simplification introduced into the aircraft dynamic model specialised for performance studies is that of considering the aircraft as a point mass. In this way, the study is limited to the motion of the aircraft's centre of gravity only, while the aircraft motions around it (e.g., in the case of disturbance response or change in equilibrium conditions) are considered negligible for overall performance. This simplification is acceptable, as a civil transport aircraft must possess stability and controllability requirements that guarantee short transients that do not affect its overall trajectory. With this simplification, the equations of the point mass aircraft are reduced to just the force equations, while the moment equations can be neglected. The forces acting on the centre of gravity are the aerodynamic actions of lift L and drag D, the weight W and the propulsive thrust T. The second simplification introduced in the aircraft dynamic model is to consider the flight performance for an aircraft whose mission trajectory

lies in the vertical plane only. Thus, the flight phases of take-off, climb, cruise, descent and approach are considered, whereas turns are neglected. The third assumption is to consider the thrust force always aligned with the aircraft velocity. The trajectory and the associated performance of an aircraft can therefore be calculated by properly time-integrating the differential equations of motion; the integration can be performed using different numerical techniques, some of which are collected and proposed in [63–67].

The coupling of a proper set of equations for the dynamics of a system (in this case, an aircraft) with the appropriate techniques for time-integration of these equations enables the definition of what is commonly intended as a simulator. In aircraft design, simulation techniques are fundamental in every step of the design and validation process of the aircraft and its systems. Indeed, by means of simulation techniques, it is possible to characterise the behaviour of the aircraft and its systems, and to adapt design choices or optimisation efforts consequently. In the literature, there are several examples in which aircraft dynamics simulation techniques have been proposed in this sense. In [68], the importance of simulation-based design is emphasised, and a detailed simulation framework is proposed to be included in the context of the overall aircraft design process. In particular, refs. [68,69] focus on simulation techniques for take-off and landing manoeuvres, to be implemented within an even broader framework of aircraft dynamic simulation, proposed in [70–72]. In [73], a simulator relating to take-off dynamics is presented, which is also able to evaluate the influence of ground effect aerodynamics, and thus to characterise the dynamic performance of aircraft with different lifting systems. The study in [74] proposes a detailed approach for simulating the flight of transport aircraft; this approach is capable of evaluating the effect of innovative controls, such as direct lift control for box-wing aircraft. A mixed technique, which aims to enhance the accuracy of simulations by incorporating real flight data, is presented in [75,76]; this model proposes improved mission performance predictions compared to physics-based models only. In [77], the complete simulation of aircraft dynamics is integrated within a multidisciplinary design and optimisation platform, with the aim, among others, of taking certification constraints into account within the design process. In [78], aircraft mission simulations are used to evaluate structural loads, and to gain information about wings' structural fatigue. Mission simulation and performance analysis techniques were also applied for the evaluation of design parameters to be optimised in the case of aircraft with innovative propulsion, as in the case of the fuel cell-powered UAV presented in [79]. Moving from aircraft to systems, simulation techniques were applied in [80,81] to evaluate on-board power management, or in [82] to integrate the effects of system/subsystem implementation into the conceptual design.

2.3.2. Mission Simulation: Aeromechanics

This section introduces the mathematical model useful for the flight simulation in the longitudinal plane of the aircraft considered as a point mass, according to the assumptions presented in Section 2.3.1. The equations are written considering the wind reference frame, while the trajectory is computed in the local vertical reference system (X_V, Z_V); the force scheme considered is reported in Figure 4.

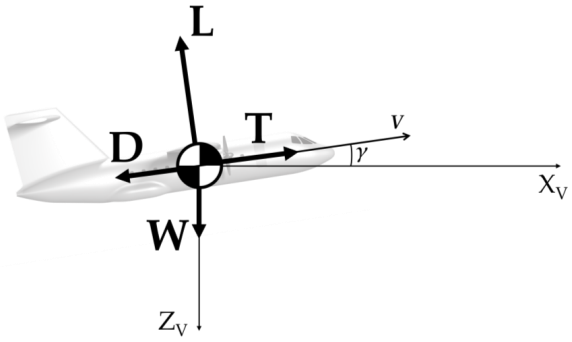

Figure 4. Force schema.

The system of aircraft dynamics equations under these assumptions becomes:

$$\begin{cases} \frac{W}{g}\dot{V} = T\text{-}D\text{-}W\sin\gamma \\ \frac{W}{g}V\dot{\gamma} = L\text{-}W\cos\gamma \\ V_x = V\cos\gamma \\ V_z = -V\sin\gamma \\ \dot{W} = -k_c P_e \end{cases} \quad (2)$$

where W is the aircraft weight, g is the gravity acceleration, V is the aircraft speed, T is the engine thrust, L is the lift, D is the drag, γ is the trajectory slope, x is the longitudinal axis, z is the vertical axis, k_c is the power-specific fuel consumption and P_e is the supplied power. All the quantities are time functions, except for g and k_c, which are constants. Dotted variables indicate the time derivative of the considered quantity. The trajectory of the aircraft and the related performance, such as fuel consumption, travel time, distance covered, etc., can be obtained by time-integrating differential Equation (2), given the initial conditions and the proper flight programmes selected for each mission phase. Specifically, in this work it was decided to use the Euler forward method as a technique for numerical integration of the equations of motion. Such a model is given in Equation (3) for a generic y function of time t; $\dot{y}$ represents the time derivative of the considered function, while Δt is the finite timestep in which the mission is discretised.

$$y(t + \Delta t) = y(t) + \dot{y}(t)\Delta t \quad (3)$$

The mission can be split into phases; in this work, it has been divided into taxi-out, take-off, climb, cruise, descent, diversion and loiter, approach, landing and taxi-in (Figure 5); the airborne phases are simulated through the dynamic model of Equation (2).

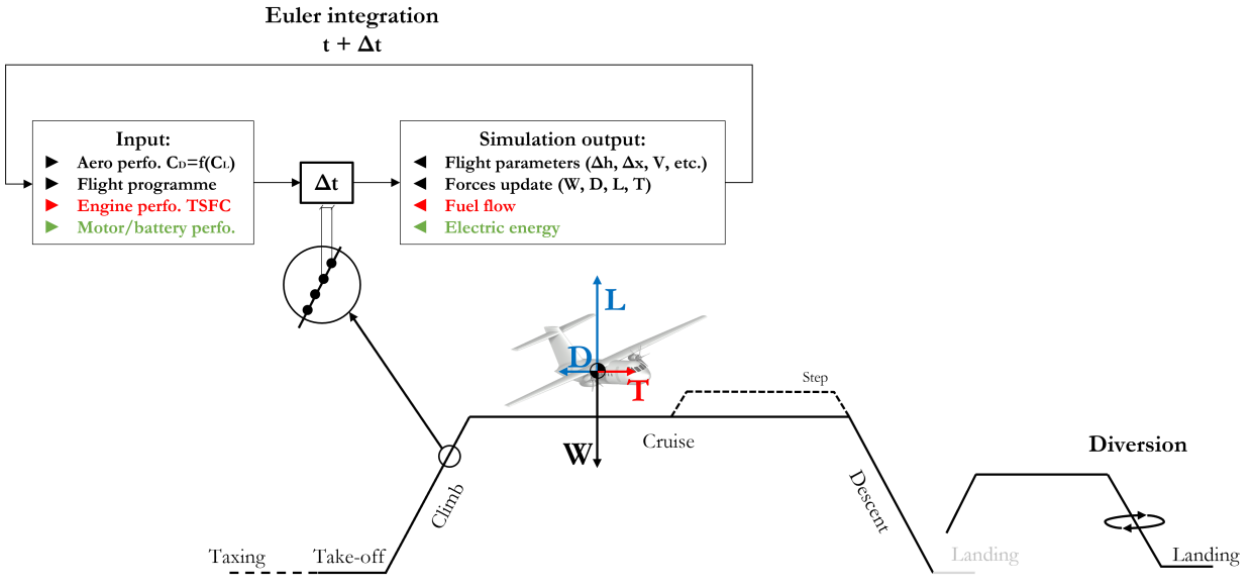

Figure 5. Scheme of the aircraft mission simulation.

For each stage, the corresponding flight programmes were selected, which when properly implemented in the simulation model allow the acquisition of all information relating to the aircraft mission performance. The following programmes were selected:

- Taxi-out: ground manoeuvring with constant power supply for 240 s;
- Take-off: full-power supply for 45 s;
- Climb: constant indicated air speed (IAS) and rate of climb (RoC);
- Cruise: constant speed and altitude;

- Descent: constant indicated air speed (IAS) and rate of descent (RoD);
- Loiter: 30 min of level flight at maximum L/D;
- Approach: constant RoD;
- Landing: neglected;
- Taxi-in: ground manoeuvring with constant power supply for 240 s.

For diversion climb, cruise and descent, the same programmes of standard mission were applied; the differences rely on the flight conditions, as summarised in Table 2.

Table 2. Conditions for the flight programmes for mission and diversion.

	Mission		Diversion	
Climb	IAS = 170 kt	RoC = 900 ft/min	IAS = 150 kt	RoC = 600 ft/min
Cruise	Mach = 0.4	h = 6100 m	Mach = 0.27	h = 3050 m
Descent	IAS = 220 kt	RoD = −1100ft/min	IAS = 150 kt	RoD = −1100ft/min

Compared to aircraft propelled by a single source of power and energy, such as conventional turboprop aircraft, hybrid vehicles require a characterisation of power supply during the mission as well. Specifically, it is necessary to determine which source of power and energy, and in which proportion, is to be provided at a given moment or phase of the mission. This aspect is discussed in Section 2.3.3.

2.3.3. Mission Simulation: Power Supply

In this work, a parallel hybrid-electric powertrain architecture was selected; with this configuration, the thermal and electrical sources can supply power to the propeller independently. The electric motor and the thermal engine are linked to the propeller by a gearbox, as schematically sketched in Figure 6.

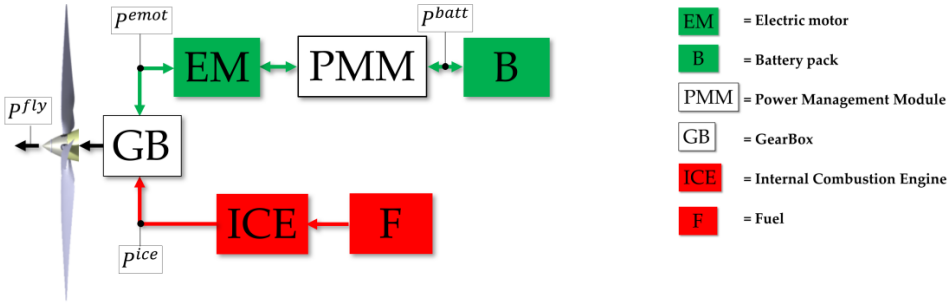

Figure 6. Scheme of the parallel hybrid-electric powertrain.

A key aspect to estimate aircraft performance is the *power management strategy* (Figure 2). Specifically, this aspect introduces a new set of design variables, related to the supply strategy of the electric and thermal power throughout the flight. These variables are the thermal power fraction Φ^{ice} and the electric power fraction Φ^{el}, defined according to Equation (4) and Equation (5), respectively, where P^{ice} is the power supplied by the thermal engine and P^{emot} is the power supplied by the electric motor. The total power fraction supplied Φ is defined according to Equation (7).

$$\Phi^{ice}(t) = \frac{P^{ice}(t)}{P^{ice}_{inst}} \tag{4}$$

$$\Phi^{el}(t) = \frac{P^{emot}(t)}{P^{emot}_{inst}} \tag{5}$$

$$\Phi(t) = \frac{P^{emot}(t) + P^{ice}(t)}{P^{emot}_{inst} + P^{ice}_{inst}} = \frac{P^{nec}(t)}{P^{tot}_{inst}} \tag{6}$$

These are key variables for properly assessing the power balance of the hybrid-electric aircraft, i.e., how the power is supplied by the thermal and electrical chains to match the power required to fly. Equation (7) characterises such a balance. Specifically, the flight required power P^{fly} must be balanced at each instant of the mission by the sum of the power supplied by the thermal chain P^{ice} and the electrical chain P^{emot}, net of the mechanical connection dissipations, expressed by the efficiencies of the gearbox η_{gear} and the propeller η_{prop}.

$$\begin{cases} P^{fly} = DV + VW\sin\gamma \\ P^{ice} + P^{emot} = \dfrac{P^{fly}}{(\eta_{gear}\eta_{prop})} = P^{nec} \end{cases} \quad (7)$$

The quantities in Equation (8) are time-dependent variables, except for the efficiencies η_{gear} and η_{prop}, which are considered constant. Considering Equations (4)–(7), given the required power P^{nec} and fixed $\Phi_i^{ice}(t)$ (or $\Phi_i^{el}(t)$, as the two terms are linearly dependent), it is possible to uniquely identify the time history of thermal power and electrical power supply throughout the mission. Acting on these variables, a given aircraft may exhibit different fuel and battery mass distributions on a specific mission. For this reason, it is necessary to clarify the choices regarding power supply variables made in this work. A simplified scheme in this respect is proposed in Figure 7. First of all, it is worth starting with a clear distinction in the power supply management strategy between standard mission and diversion. A basic assumption has been posed in this regard: batteries can be used only in a standard operating mission, whereas the diversion is accomplished by using thermal power only. Indeed, since diversion rarely occurs, but its energy/power request needs to be taken into account for each mission considered, this assumption avoids carrying a large unused battery mass on board, which could have detrimental effects on the overall aircraft performance without benefits in emissions reduction.

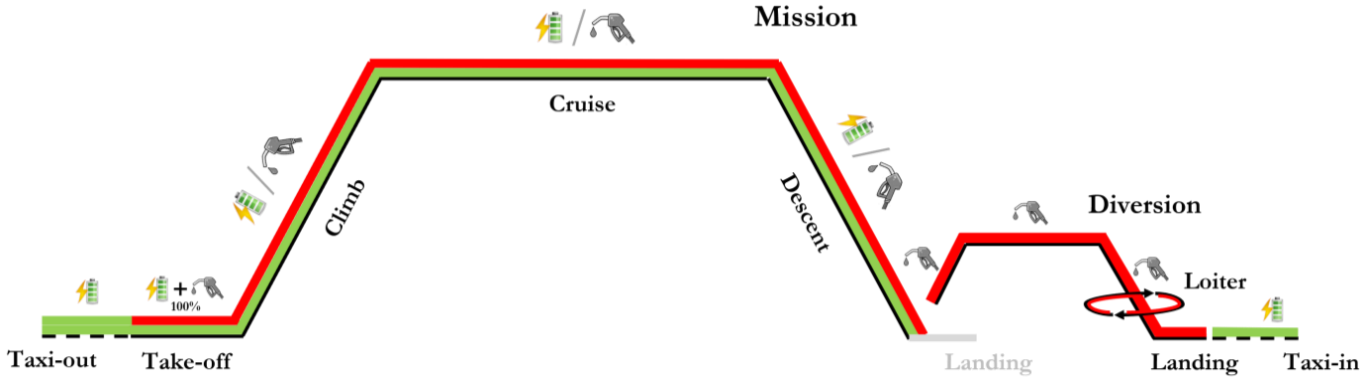

Figure 7. Mission profile with a scheme of the selected power supply strategy.

With regard to the standard operating mission, the following considerations have been made for the different mission phases:

- Taxi-out/Taxi-in: taxiing is performed with only electrical power supply, in order to suppress all air-polluting emissions on the ground;
- Take-off: all the available power on board, both electrical and thermal, is supplied;
- Climb, Cruise, Descent: for each phase, electrical and thermal power are supplied in different quotas to match the total power required for the flight, according to a strategy set by the designer/operator.

In this study, the selection of the power supply strategy in the climb, cruise and descent phases was carried out by means of an optimisation procedure. In particular, since the main purpose of hybrid-electric aircraft development lies in the possible reduction of greenhouse gas emissions, the optimisation was set to minimise block fuel. The tool used to design the hybrid-electric aircraft and to evaluate the objective function within

the optimisation procedure was THEA-CODE (Section 2.2). The optimisation problem is described by Equation (8).

$$\begin{cases} \textit{objective function} \\ \quad \min(m_{\text{block fuel}}(\mathbf{x})) \\ \\ \textit{design space} \\ \quad W/S_{min} < W/S < W/S_{max} \\ \quad 0 < H_P < H_{Pmax} \\ \quad 0 < \Phi_i^{ice} < \Phi_{max}^{ice} \\ \\ \textit{constraints} \\ \quad MTOW(\mathbf{x}) \leq MTOW_{max} \\ \quad \Phi_i^{el} \leq \Phi_{max}^{el} \end{cases} \tag{8}$$

The optimisation design variables **x** are those related to the sizing of the propulsion system by means of a matching chart, i.e., the wing loading W/S and the hybridisation factor H_P, and those related to the power supply strategy Φ. As described above, at each time, given the total required power P^{nec}, it is sufficient to identify the fraction of supplied thermal power to also know the electric power fraction, or vice versa. In this case, it was chosen to select the thermal power fractions Φ_i^{ice} for the three *i-th* phases (climb, cruise, descent) as optimisation variables, and to compute the electrical power fractions Φ_i^{el} accordingly. Furthermore, since the power fractions Φ_i are functions of time, a further simplifying assumption was imposed: the thermal power fractions, used as optimisation variables, are kept constant within the *i-th* phase considered, while the electrical power fractions can vary over time in the *i-th* phase, depending on the matching with the total required power. A summary overview of the choices related to the power supply strategy is given in Table 3.

Table 3. Designer assumptions on supplied power fractions.

		Thermal Power Fraction	Electric Power Fraction
Mission	**Taxi-out/in**	$\Phi^{ice}(t) = 0$	$\Phi^{el}(t) = 0.07\ P_{inst}^{tot}$
	Take-off	$\Phi^{ice}(t) = 1$	$\Phi^{el}(t) = 1$
	Climb	$\Phi^{ice}(t) = \text{const.} = \Phi_{climb\ opt}^{ice}$	$\Phi^{el}(t) = f(\Phi(t),\ \Phi_{climb\ opt}^{ice})$
	Cruise	$\Phi^{ice}(t) = \text{const.} = \Phi_{cruise\ opt}^{ice}$	$\Phi^{el}(t) = f(\Phi(t),\ \Phi_{cruise\ opt}^{ice})$
	Descent	$\Phi^{ice}(t) = \text{const.} = \Phi_{desc\ opt}^{ice}$	$\Phi^{el}(t) = f(\Phi(t),\ \Phi_{desc\ opt}^{ice})$
Diversion	$\mathbf{Climb_{div}}$	$\Phi^{ice}(t) = \Phi(t)$	$\Phi^{el}(t) = 0$
	$\mathbf{Cruise_{div}}$	$\Phi^{ice}(t) = \Phi(t)$	$\Phi^{el}(t) = 0$
	$\mathbf{Descent_{div}}$	$\Phi^{ice}(t) = \Phi(t)$	$\Phi^{el}(t) = 0$

The optimisation problem is completed with a set of constraints; in this case, a maximum limit is imposed on the maximum take-off weight MTOW and on the maximum fraction of electrical power that can be supplied. The latter is set so that the electric motors do not exceed their maximum continuous power output, thus avoiding overheating issues. The optimisation problem is addressed by means of a multistart procedure coupled with local minimum gradient search algorithms, as described in [52].

3. Hybrid-Electric Aircraft Performance Analysis

3.1. Analysis of the Design Mission Performance

This section presents the performance analysis at the design point of a regional hybrid-electric aircraft sized according to the methods proposed in Section 2.2, to meet the require-

ments defined in Table 1 (Section 2.1). The main characteristics of this configuration are proposed in Table 4, while the sketch of its planform is shown in Figure 8. As THEA-CODE is not conceived to redesign the geometry of the lifting system, the planform optimisation was performed by means of the aerodynamic optimiser AEROSTATE [83]; this code can modify the input lifting system geometry to maximise the cruise lift-to-drag ratio while satisfying the constraints of static stability and trim in the longitudinal plane.

Table 4. Main parameters of the regional hybrid-electric aircraft.

Number of Passengers	40
Design range	600 nm
MTOW	22,935 kg
OEW	17,879 kg
Wing surface	70.6 m^2
Wingspan	28.7 m
Fuselage length	21.9 m
Fuselage diameter	2.88 m
Installed thermal power	3.21 MW
Installed electric power	2.49 MW
H_P	0.43
Block fuel mass	937 kg
Battery mass	4054 kg

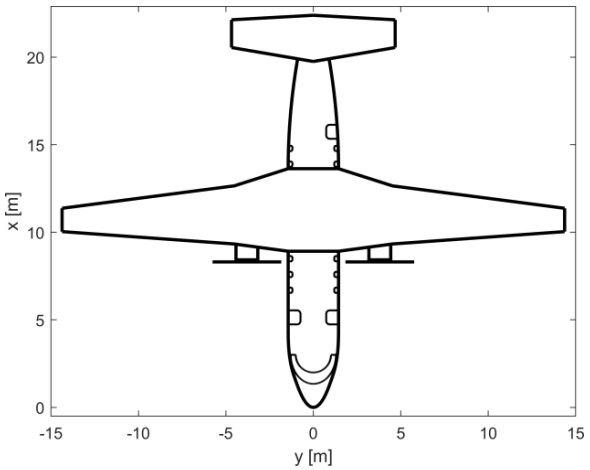

Figure 8. Planform of the hybrid-electric regional aircraft.

Figure 9 shows the main outcomes of the simulation set-up described in Section 2.3; in particular, the aircraft trajectory (left), the trajectory slope angle γ (centre) and the lift-to-drag ratio L/D (right) are shown.

Figure 10 depicts the time evolutions of the power supplied by the thermal and electrical chains, both in absolute terms and in power fractions Φ. The results of the optimisation, consistently with the designer's strategy for power management during the mission, represent the best way to exploit on-board electrical power to minimise fuel consumption, for this specific case study.

Figure 11 shows the results in terms of fuel and battery mass required to complete the individual phases into which the mission was divided. The optimiser finds solutions to utilise as much electrical energy as possible in the most energy-intensive phases of the mission, i.e., climb and cruise. The limit to this is set by the constraint on $MTOW_{max}$, which

restricts the maximum amount of batteries that can be taken on board. In line with the requirement set by the designer, there is no use of electrical energy in diversion.

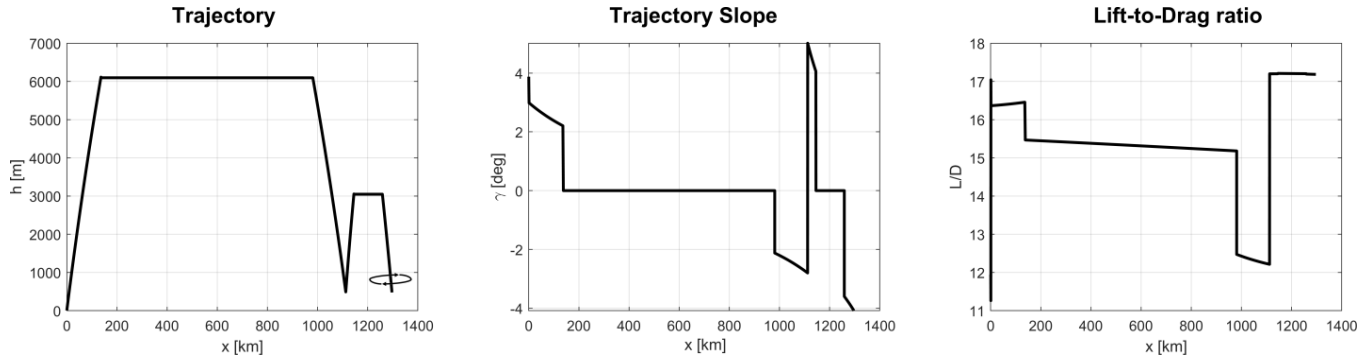

Figure 9. Mission simulation outcomes: trajectory (**left**), slope angle (**centre**), lift–drag ratio (**right**).

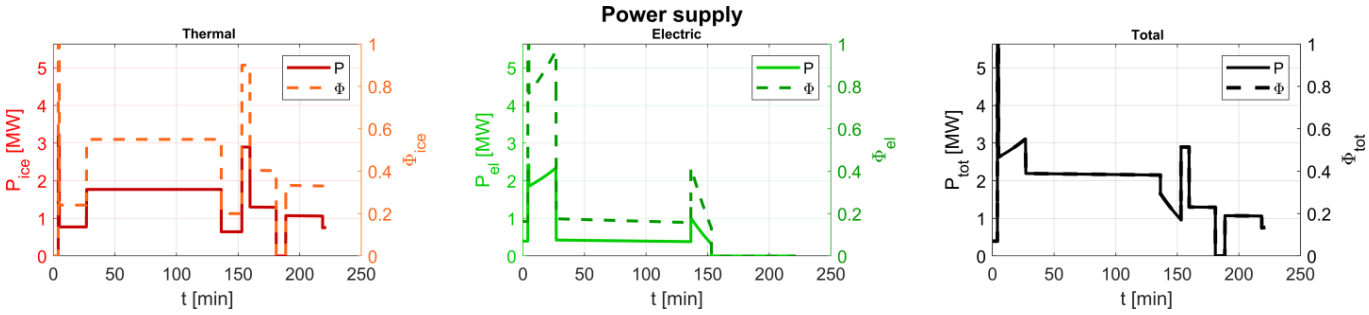

Figure 10. Mission simulation outcome: thermal (**left**), electric (**centre**), total (**right**) power supplied.

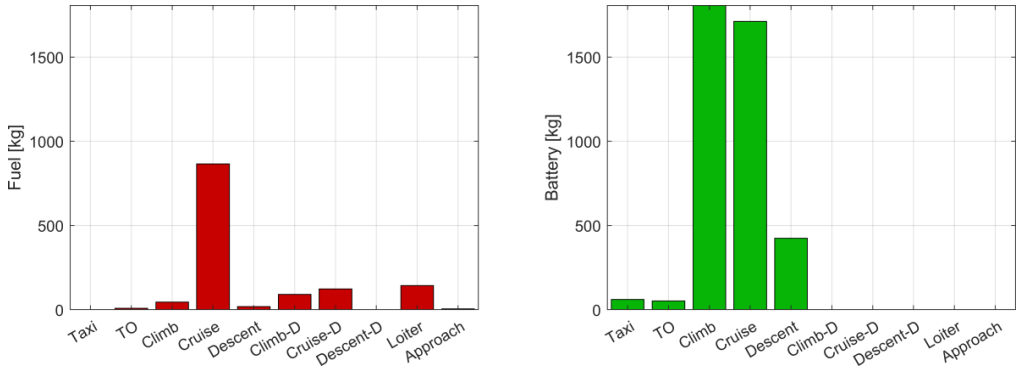

Figure 11. Mission simulation outcome: fuel (**left**) and battery (**right**) mass breakdown.

3.2. Analysis of the Off-Design Mission Performance

During aircraft development, the design-steering figures of merit are evaluated at specific design points, typically specified in the top-level design requirements. However, the typical operating conditions of the aircraft are different from those provided by the specification, as in practical use a variety of combinations of payload, mission range, fuel (and/or battery) weight and hence take-off weight may occur. A novel aircraft, therefore, must prove to have a wide operational flexibility. In general, the term flexibility refers to the capability of a system to satisfactorily meet requirements that differ from the reference operating conditions [84]. For a transport aircraft, this implies the capability of the vehicle to fly efficiently in the widest range of off-design missions, in terms of mission profile (e.g., speed, altitude), but more importantly in terms of combinations of payload and flight distances [85]. In this section, an example of performance evaluation for off-design missions of the hybrid-electric regional aircraft described in Section 3.1 is proposed. For

these analyses, the payload was varied from 20 to 40 passengers, while the flight distances ranged from 250 to 600 nm. The pax–range diagram was constrained at the top by the design point mission, defined by the top-level requirements reported in Table 1. The performance trends are shown inside the payload–range envelope, in terms of block fuel, battery mass and take-off mass, highlighting any possible general difference with respect to the thermally powered aircraft.

A converger for the setting up of the supplied power fractions was used to assess this performance analysis. This procedure was adopted to avoid the huge increase in computation time there would have been if we had used an optimisation procedure for each point inside the pax–range envelope. Specifically, the converger strategy aims to reduce the block fuel consumption, by supplying the maximum available electric power during climb and cruise, and compensating any excess of requested power with the thermal one. In other terms, the goal of this strategy is to maintain the values of Φ^{el}_{climb} and Φ^{el}_{cruise} as close as possible to their available maximum. Following this strategy, any increase in the energy demand for flight, due, for example, to a larger payload or a longer range, implies an increment in the requested electric energy, leading to heavier battery packs; when this increment results in the condition $W_{TO} > MTOW$, the Φ^{el} values have to be reduced and the power request has to be fulfilled, increasing the supplied thermal power. This causes a lighter battery pack and hence the fulfilment of the MTOW constraint, including for the most energy-demanding passengers–range combinations. The thermal and electric power fractions found with this strategy, for each payload–range pair evaluated, are reported in Figure 12. As in the case of the design point, in this case the Φ^{ice} are also constant within each phase, whereas Φ^{el} are time variables, depending on $\Phi(t)$; so, at the bottom of Figure 12, the values of Φ^{el} at the beginning of the climb (left) and cruise (right) are reported.

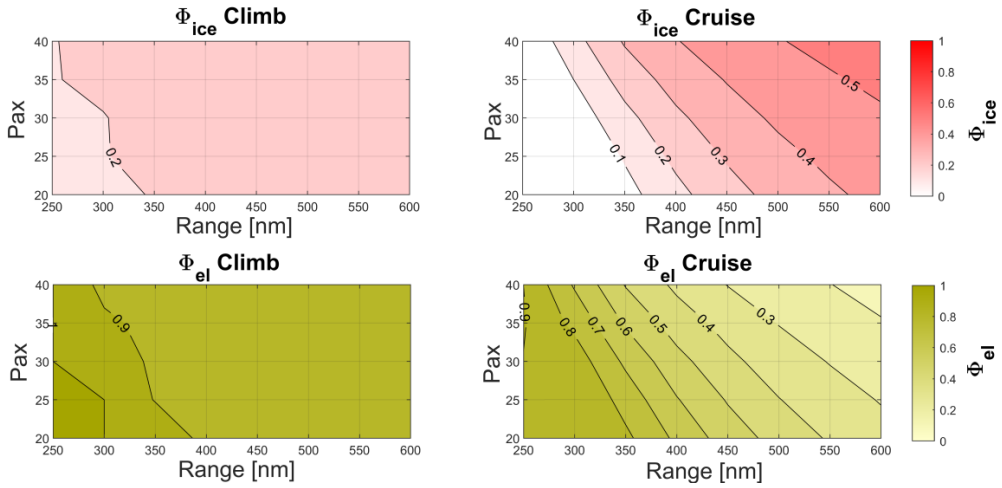

Figure 12. Thermal (**top**) and electrical (**bottom**) supplied power fractions in climb (**left**) and cruise (**right**) for the missions inside the pax–range diagram.

Figure 13 shows the trends of block fuel (left) and battery mass (centre) required for the missions inside the pax–range diagram of the reference aircraft, together with the related take-off weight W_{TO} (right). The trend of fuel consumption basically follows the trend of thermal power fraction supplied in cruise (Figure 12—top right). When the energy demand of the assessed mission decreases, i.e., as the payload and/or range decreases, it is possible to exploit a larger supply of electrical power (Figure 12—bottom right), thus allowing reduction of the fuel consumption. In a 40-passenger 250 nm mission, which can be considered the mission of typical use of this class of aircraft [50], it can be seen that the fuel consumption becomes very limited (approximately 50 kg), thus favouring a significant reduction in direct emissions from the operation of such an aircraft.

The battery mass shows some interesting trends (Figure 13—centre); first, in the area of the pax–range envelope where fuel consumption is below 100 kg, the battery mass

gradually increases as the range increases. The increasing trend stops when the take-off weight W_{TO} reaches the MTOW value; beyond this line, the MTOW cannot be exceeded (Figure 13—right), and it is necessary to swap battery mass for fuel mass in order to accomplish the missions. This is carried out by increasing the thermal power fraction and reducing the electric power fraction in cruise, as Figure 12 (right) shows. In contrast to the conventional thermal aircraft, for which the W_{TO} = MTOW condition only occurs on one point of the diagram edge, in this case a large area within the envelope is subject to this condition (Figure 13—right). In this area of the envelope, once the payload is fixed, the gradual mass exchange between batteries and fuel occurs.

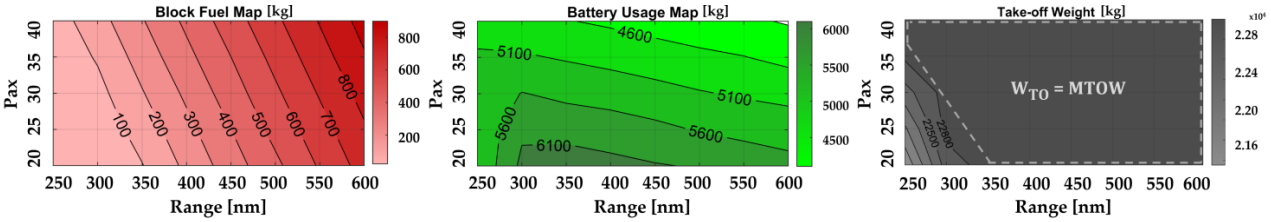

Figure 13. Block fuel (**left**), battery mass (**centre**), and take-off weight W_{TO} (**right**) for the missions inside the pax–range diagram.

4. Beyond the Design Point: Payload–Range Diagram Analysis

The broader the operating flexibility, the greater the relevance of the new aircraft in the air transport market. In the following sections, the main differences between the operating flexibility of an aircraft with conventional thermal propulsion and one with hybrid-electric propulsion are described. To support these investigations, the complete payload–range diagram is consistently used.

4.1. Payload–Range Diagram for Aircraft with Thermal Propulsion

A qualitative step-by-step description of the payload–range diagram for aircraft with thermal propulsion is provided in this section in order to better explain the differences from hybrid-electric aircraft. Figure 14 shows the first part of the diagram, where the x-axis is the flight range, and the y-axis is the difference between the aircraft weight and the empty operating weight (W_{eo}), which is constant and therefore subtracted from the total aircraft weight, for simplicity. The weight contributions represented in Figure 14 are: (i) the payload weight W_{pay}; (ii) the fuel weight W_{fuel}, which has the origin starting from the maximum value of the payload weight ($W_{pay\ max}$); (iii) the aircraft take-off weight W_{TO}, i.e., the sum of payload, fuel and empty operating weight, limited at the top by the maximum take-off weight MTOW. Once the payload weight is set equal to its maximum, the fuel weight required to accomplish the mission is the key factor which determines the take-off weight of the aircraft; W_{fuel} depends on the aerodynamic, ponderal and propulsive characteristics of the aircraft, and it assumes a distinct value for each range considered. Therefore, there is a monotonically increasing correlation between the W_{TO} and the flight range, which is valid up to the so-called *harmonic point* [86], at which the take-off weight reaches the MTOW limit. This point of the payload–range diagram indicates the maximum range the aircraft can fly with the maximum payload, i.e., the harmonic range (R_H).

To increase the flight distance beyond the harmonic range, it is necessary to reduce the payload mass, allowing an equivalent increase in fuel mass, as shown in Figure 15 (left). Note that the origin of the y-axis related to the W_{fuel} "slides" on the $W_{pay\ max}$ line, thus giving a concise and general interpretation of this diagram. In this segment of the envelope, the take-off weight of the aircraft W_{TO} is always equal to the maximum weight MTOW.

The trend depicted in Figure 15 (left) stops once the maximum volume available in the tanks is saturated; from this point on, it is no longer possible to increase the fuel mass on board. Therefore, in order to achieve increases in flight range, it is necessary to reduce the payload weight further to obtain a lighter aircraft; the fuel weight is kept constant, equal to $W_{fuel\ max}$, as represented in Figure 15 (right). When the payload weight

decreases to zero, the aircraft reaches its maximum range, defined as *ferry range*. This situation is of minor commercial interest, unless for the conditions of aircraft delivery or transfer. Figure 15 (right) thus represents the complete generic payload–range diagram for an aircraft with conventional thermal propulsion. The edge of the envelope represents the limiting conditions in terms of payload maximisation; all the combinations within the envelope are feasible missions for the considered aircraft.

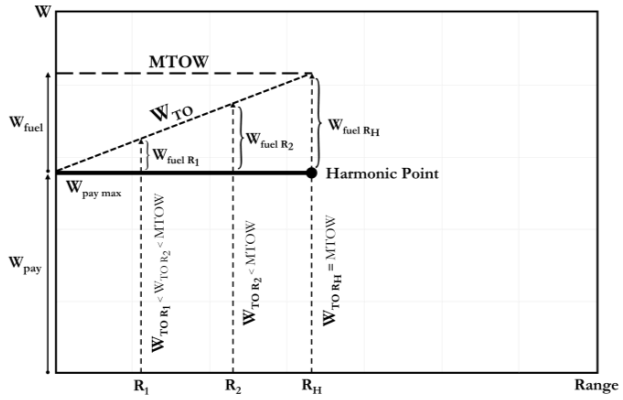

Figure 14. Payload–range diagram for aircraft with thermal propulsion—Part 1.

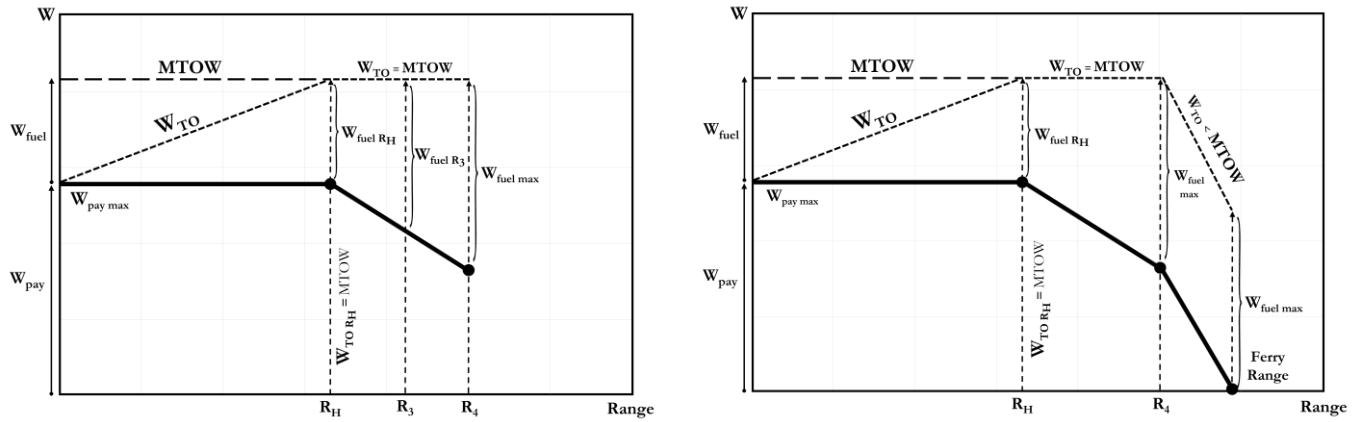

Figure 15. Payload–range diagram for a conventional thermal powered aircraft—Part 2.

4.2. Payload–Range Diagram for Aircraft with Hybrid-Electric Propulsion

Aircraft propelled by a dual source of power and energy show different operating performances which are reflected in the payload–range diagram; the aircraft considered here is equipped with a parallel hybrid-electric powertrain. Compared to the thermal propulsion case, the first clear difference can be observed in the y-axis of the diagrams in Figure 16: the hybrid-electric aircraft has an additional item, the mass of the batteries. Therefore, the W_{TO} depends on the fuel–battery mass distribution, depending on the split of the power supply during the different stages of the mission; Figure 16 provides a qualitative clarification of this point. In Figure 16 (left) (*Case 1*), the strategy adopted is targeted at maximising the mass of batteries on board; due to the low energy density of the batteries, W_{TO} reaches the MTOW limit well before the harmonic point. On the other hand, in the case of Figure 16 (right) (*Case 2*), a different fuel–battery mass distribution is adopted, in which a higher fuel consumption is allowed. In this instance, W_{TO} reaches the MTOW for a longer range than in the previous case.

To increase the aircraft range while maintaining the maximum payload and fulfilling the MTOW constraint, it is necessary to reduce the battery mass and compensate the required energy demand by increasing the fuel mass, as shown qualitatively in Figure 17. The gravimetric densities of the two energy sources are very different from each other, so the

mass variation of each of them with range has different absolute values, as the slopes of the dashed red and green lines in Figure 17 show. In this segment, differently from the thermal aircraft, the condition W_{TO} = MTOW always occurs. This segment should end at the harmonic point, which is defined as the point with the maximum range for the maximum payload, and where W_{TO} equals MTOW for the first time. This definition of *harmonic point* is clearly no longer valid in the case of hybrid-electric aircraft; it is therefore more consistent to generically identify this point as the *design point*, i.e., the point that, according to the specifications, sets the requirements to size and/or op-528 timise the aircraft.

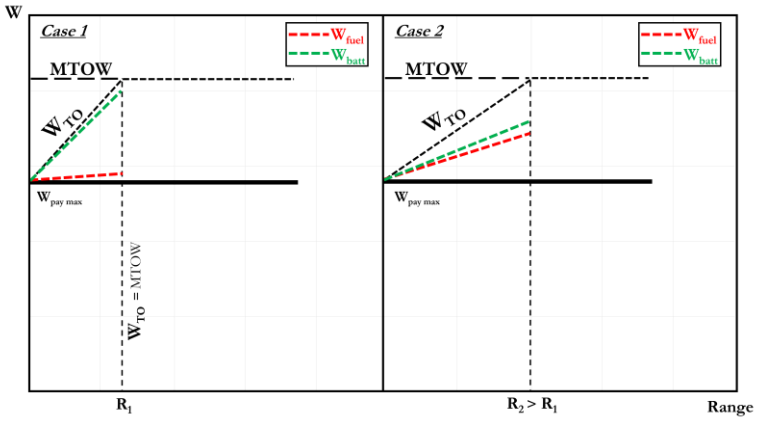

Figure 16. Effects of different fuel–battery mass distributions on the first segment of the payload–range diagram for hybrid-electric aircraft.

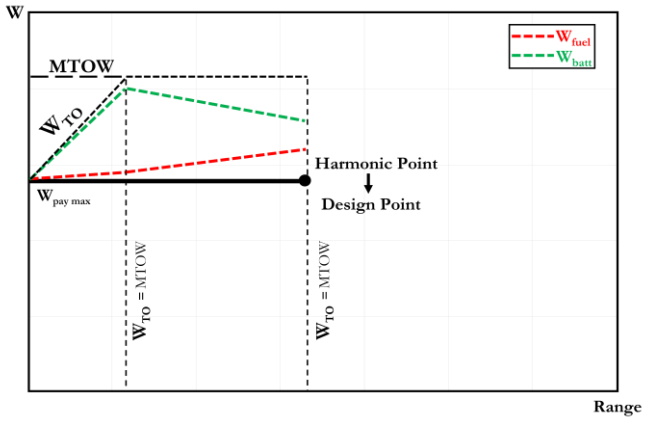

Figure 17. Payload–range diagram for hybrid-electric aircraft—Part 1.

The most important difference between conventional thermal aircraft and hybrid-electric aircraft is how to manage the operations beyond the design point. In fact, in the case of aircraft with thermal propulsion, beyond the harmonic point it is only possible to exchange fuel and payload mass to increase the range and meet the MTOW constraint. In the case of dual energy aircraft there are at least three different strategies to increase the range beyond the design point, as described hereafter. It is worth highlighting that the different strategies described in the following are qualitative; specific constraints, such as those on the maximum available power, both electrical and thermal, must always be fulfilled for the specific aircraft and the related missions considered.

The first strategy consists in exchanging payload mass for fuel mass, while keeping the battery mass constant. The payload decreases as fuel mass increases until the maximum available volume in the tanks is reached, as shown in Figure 18 (left). In this segment, the W_{TO} = MTOW condition is maintained. In the second strategy, the payload mass is exchanged for battery mass, while the fuel mass is kept constant. In this case, the battery mass increases until the maximum volume available for the batteries is saturated

(Figure 18—right). Since the gravimetric energy density of batteries is about 25 times lower than fuel, the range for which the volume saturation is achieved could be significantly anticipated. Figure 18 shows a qualitative comparison between these two strategies: given the low gravimetric energy density of batteries compared to fuel, the second strategy does not appear to be effective in extending the range; however, it may be suitable if cutting the fuel consumption is the priority.

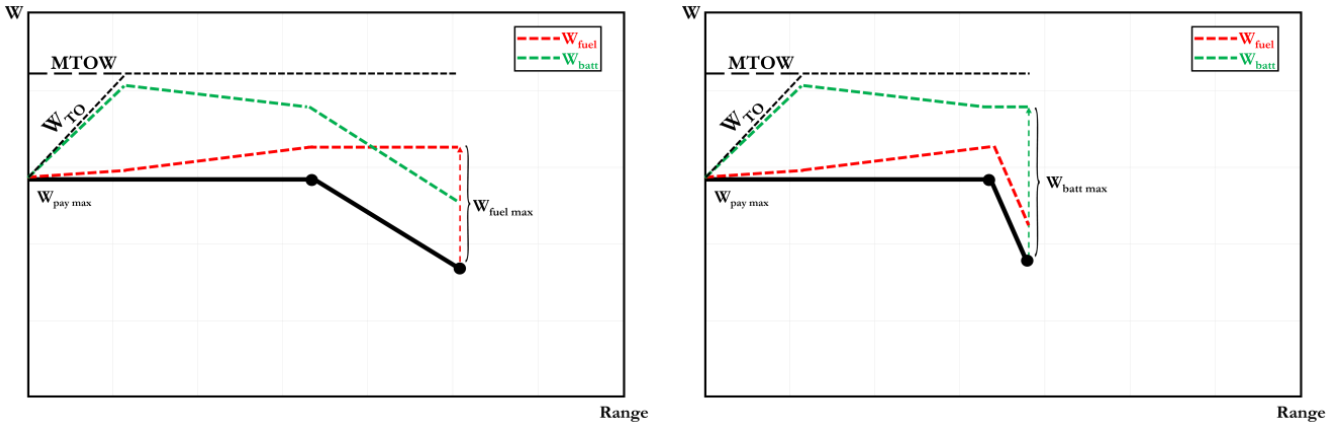

Figure 18. Strategies to extend the range beyond the design point: mass exchange between payload and fuel (**left**), and between payload and batteries (**right**).

In the third strategy, battery mass is exchanged for fuel mass, while the payload mass is kept constant and equal to $W_{pay\ max}$ (Figure 19). As fuel has a much higher gravimetric energy density than batteries, very large design range extensions could be obtained.

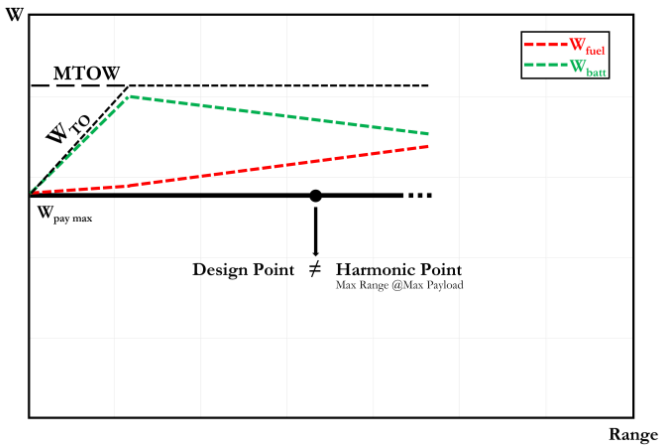

Figure 19. Strategy to extend the range beyond the design point: batteries and fuel mass swap.

Using this strategy, it is necessary to define what is the maximum range extension achievable with the maximum payload, starting from the *design point* D_P. The maximum range, defined in the following as *extended range* E_R, depends on the specific characteristics of the aircraft and the propulsion system; in particular, following the diagrams in Figure 20, in which qualitative details of the payload–range diagrams in the area beyond the design point are represented, the following cases occur:

- *Case 1*: the extended range is limited by the saturation of the maximum volume available for fuel; this depends on the design of the aircraft, in particular on the allocation of internal volumes for fuel and/or batteries.
- *Case 2*: the extended range is limited because the MTOW is reached, no further battery–fuel mass swap is possible, hence it is necessary to start reducing the payload.

- *Case 3*: the extended range is limited by the lack of available energy or power, which depends on the sizing of the propulsion system and in particular on the hybridisation factor. Two subcases are possible:
  - *3a*: electrical energy is not sufficient to accomplish one or more stages of the mission;
  - *3b*: the power provided by the thermal engine is not sufficient to accomplish one or more mission stages.

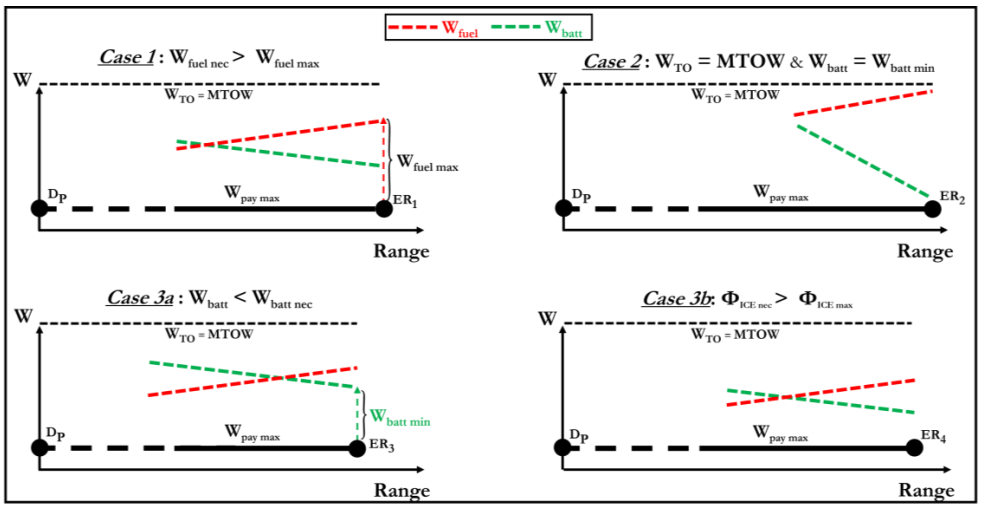

Figure 20. Four different scenarios to define the extended range.

The most restrictive constraint sets the limit on the maximum range achievable with the maximum payload.

The general qualitative framework described above is supported in the following by a quantitative analysis of the performance of hybrid-electric aircraft. To better clarify the possibility to enlarge the operating envelope beyond the design point, and to show how the most restrictive constraint influences the *extended range* (Figure 20), two different hybrid-electric regional aircraft are compared; the main features of the two configurations are reported in Table 5. The first configuration is the same as that analysed in Section 3, and is here labelled as Φ^{ice} *limited*, as it shows a cruise thermal supplied power fraction $\Phi^{ice}_{cruise\ opt}$ near to the maximum available value Φ^{ice}_{max}. This condition is representative of *Case 3b* of Figure 20. The second regional hybrid-electric configuration has also been designed by means of the tools described in Section 2.2; this aircraft is here labelled as *Swap limited*, and is representative of *Case 2* of Figure 20.

Table 5. Hybrid-electric aircraft main characteristics.

Design Point Features	Φ^{ice} *Limited*	*Swap Limited*
H_P	0.43	0.27
$\Phi^{ice}_{climb\ opt}$	0.28	0.37
$\Phi^{ice}_{cruise\ opt}$	0.55	0.33
$\Phi^{ice}_{desc\ opt}$	0.20	0.53
MTOW	22,935 kg	22,960 kg
Installed thermal power	3.21 MW	4.39 MW
Installed electric power	2.49 MW	1.67 MW
Block fuel mass	937 kg	1041 kg
Battery mass	4054 kg	4065 kg

Figures 21 and 22 show the performance of the two hybrid-electric aircraft inside their complete payload–range envelope, thus also considering the range extension beyond the design point. For both, the third strategy has been used to extend the aircraft range (mass swap between battery and fuel). Figure 21 reports block fuel, battery and take-off weight for the Φ^{ice} *limited* configuration. The cruise-required thermal power saturates its allowed maximum for ranges slightly larger than the design range, thus limiting the *extended range* to 800 nm; the *ferry range* is about 1500 nm.

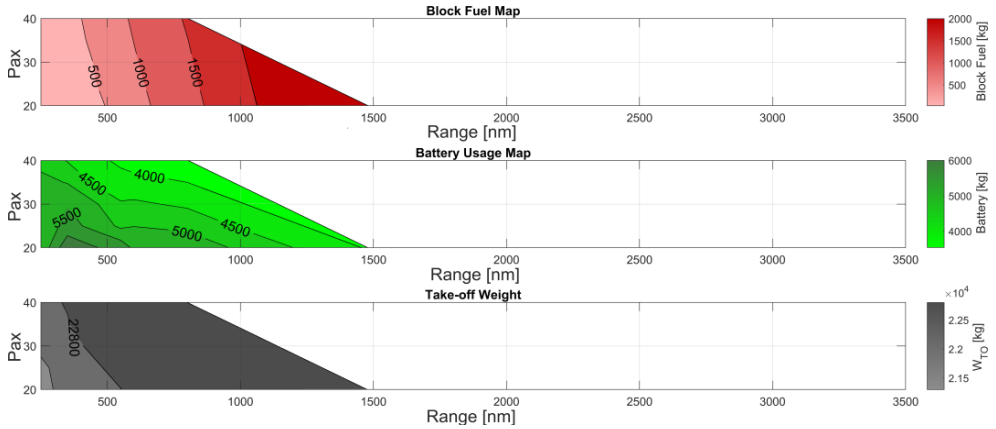

Figure 21. Fuel, battery and take-off mass trends in the whole pax–range diagram (Φ^{ice} *limited*).

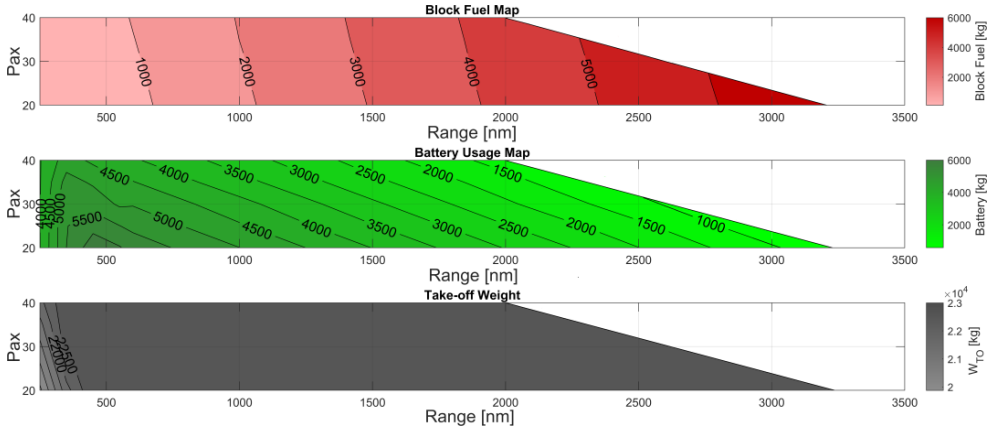

Figure 22. Fuel, battery and take-off mass trends in the whole pax–range diagram (*Swap limited*).

Figure 22 shows block fuel, battery and take-off weight for the *Swap limited* configuration. The required power constraints are always satisfied within the envelope; the *extended range* is reached when W_{TO} = MTOW and no further battery–fuel mass swap is possible. In this case, the *extended range* is equal to 2000 nm, and the *ferry range* is about 3200 nm. The mass swap between batteries and fuel allows an extension of the maximum range of the aircraft beyond the design point. Essentially, this is caused by the large amount of battery mass that can be exchanged for fuel, whose specific energy is one order of magnitude higher. Consequently, this improved operating flexibility comes at the cost of a higher fuel consumption.

To summarise, hybrid-electric parallel powertrains offer multifaced possibilities to exploit the dual energy/power sources. On the one hand, taking on board large quantities of batteries can favour the reduction of fuel consumption and direct emissions at the cost of shorter ranges; on the other hand, exchanging battery mass with fuel mass allows for significant extensions of the aircraft operational envelope. The optimisation of power supply strategy and the on-board energy management allows achievement of different performance targets: the same aircraft is able to provide "green" operations when operated

in its typical missions, and at the same time can extend its travel offer by exhibiting a much larger range compared to the typical utilisation (Figure 23).

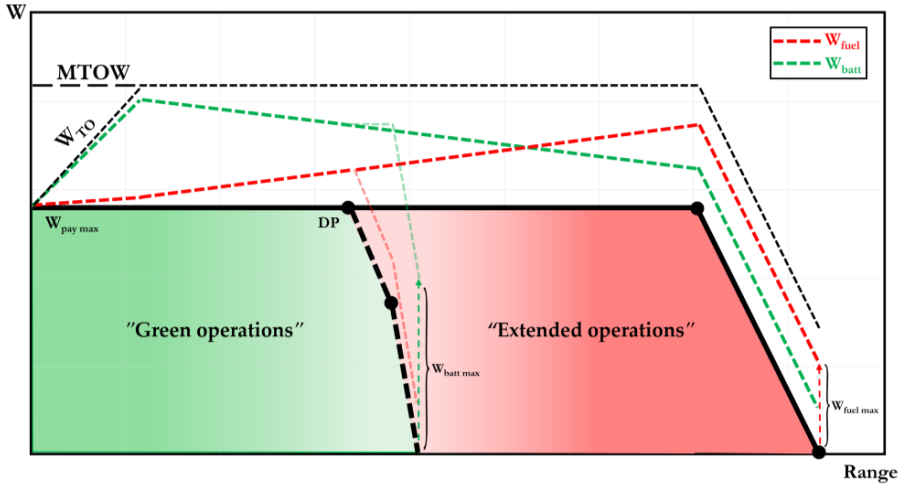

Figure 23. *Extended operations* shape for the payload–range diagram of a hybrid-electric aircraft.

5. Conclusions

In this paper, the performance analysis of regional aircraft with hybrid-electric propulsion was presented and discussed. This analysis was conducted by means of mission simulation, by specialising the dynamic model of the aircraft considered as a point mass to the mission performance study. The results show that hybrid-electric aircraft equipped with powertrains with parallel architecture present peculiar characteristics that differ from those of conventional thermal aircraft of the same category. First of all, the regional hybrid-electric aircraft shows considerable potential in terms of fuel consumption reductions; this becomes decisively relevant when considering short missions (around 250 nm), which are typical and more frequent in the utilisation of this class of aircraft. This makes this technological solution relevant in the decarbonisation path of the regional aviation category. Secondly, it has been seen that, by properly assessing the management of on-board energy sources, it is possible to obtain extensions, even substantial, of the aircraft operational envelope in terms of maximum possible flight distances. This offers much greater aircraft operational flexibility.

To improve this research, possible further developments may concern the depth of the investigations about the power management split and supply strategies throughout the mission. In particular, handling the supplied power fractions as time-varying continuous functions, and setting up ad hoc optimisation procedures, could allow achievement of lower fuel consumption than that obtained with the phase-split mission discretisation used in this work.

Author Contributions: The authors contributed equally to this work. All authors have read and agreed to the published version of the manuscript.

Funding: This research received no external funding.

Data Availability Statement: The data presented in this study are available on request from the corresponding author.

Conflicts of Interest: The authors declare no conflict of interest.

References

1. Lee, D.S.; Fahey, D.W.; Forster, P.M.; Newton, P.J.; Wit, R.C.N.; Lim, L.L.; Owen, B.; Sausen, R. Aviation and global climate change in the 21st century. *Atmos. Environ.* **2009**, *43*, 3520–3537. [CrossRef] [PubMed]
2. Parker, R. From blue skies to green skies: Engine technology to reduce the climate-change impacts of aviation. *Technol. Anal. Strat. Manag.* **2009**, *21*, 61–78. [CrossRef]

3. Brooker, P. Civil aircraft design priorities: Air quality? Climate change? Noise? *Aeronaut. J.* **2006**, *110*, 517–532. [CrossRef]
4. European Commission. *Reducing Emissions from Aviation*; on-line documentation; European Commission location: Brussels, Belgium, 2021. Available online: https://ec.europa.eu/clima/eu-action/transport-emissions/reducing-emissions-aviation_en (accessed on 15 January 2023).
5. Abbas, A.; de Vicente, J.; Valero, E. Aerodynamic technologies to improve aircraft performance. *Aerosp. Sci. Technol.* **2013**, *28*, 100–132. [CrossRef]
6. Cavallaro, R.; Demasi, L. Challenges, Ideas, and Innovations of Joined-Wing Configurations: A Concept from the Past, an Opportunity for the Future. *Prog. Aerosp. Sci.* **2016**, *87*, 1–93. [CrossRef]
7. Bravo-Mosquera, P.D.; Catalano, F.M.; Zingg, D.W. Unconventional aircraft for civil aviation: A review of concepts and design methodologies. *Prog. Aerosp. Sci.* **2022**, *131*, 100813. [CrossRef]
8. Okonkwo, P.; Smith, H. Review of evolving trends in blended wing body aircraft design. *Prog. Aerosp. Sci.* **2016**, *82*, 1–23. [CrossRef]
9. Abu Salem, K.; Cipolla, V.; Palaia, G.; Binante, V.; Zanetti, D. A physics-based multidisciplinary approach for the preliminary design and performance analysis of a medium range aircraft with box-wing architecture. *Aerospace* **2021**, *8*, 292. [CrossRef]
10. Bravo-Mosquera, P.D.; Cerón-Muñoz, H.D.; Catalano, F.M. Design, aerodynamic analysis and optimization of a next-generation commercial airliner. *J. Braz. Soc. Mech. Sci. Eng.* **2022**, *44*, 609. [CrossRef]
11. Khandelwal, B.; Karakurt, A.; Sekaran, P.R.; Sethi, V.; Singh, R. Hydrogen powered aircraft: The future of air transport. *Prog. Aerosp. Sci.* **2013**, *60*, 45–59. [CrossRef]
12. Rao, A.G.; Yin, F.; Werij, H.G. Energy Transition in Aviation: The Role of Cryogenic Fuels. *Aerospace* **2020**, *7*, 181. [CrossRef]
13. Chiaramonti, D. Sustainable Aviation Fuels: The challenge of decarbonization. *Energy Procedia* **2019**, *158*, 1202–1207. [CrossRef]
14. Magrini, A.; Benini, E.; Yao, H.-D.; Postma, J.; Sheaf, C. A review of installation effects of ultra-high bypass ratio engines. *Prog. Aerosp. Sci.* **2020**, *119*, 100680. [CrossRef]
15. Hendricks, E.; Tong, M. Performance and weight estimates for an advanced open rotor engine. In Proceedings of the 48th AIAA/ASME/SAE/ASEE Joint Propulsion Conference & Exhibit, Atlanta, GA, USA, 30 July–1 August 2012. [CrossRef]
16. Brelje, B.J.; Martins, J.R. Electric, hybrid, and turboelectric fixed-wing aircraft: A review of concepts, models, and design approaches. *Prog. Aerosp. Sci.* **2018**, *104*, 1–19. [CrossRef]
17. Sahoo, S.; Zhao, X.; Kyprianidis, K. A Review of Concepts, Benefits, and Challenges for Future Electrical Propulsion-Based Aircraft. *Aerospace* **2020**, *7*, 44. [CrossRef]
18. Schäfer, A.W.; Barrett, S.R.H.; Doyme, K.; Dray, L.M.; Gnadt, A.R.; Self, R.; O'Sullivan, A.; Synodinos, A.P.; Torija, A.J. Technological, economic and environmental prospects of all-electric aircraft. *Nat. Energy* **2019**, *4*, 160–166. [CrossRef]
19. Geiß, I.; Voit-Nitschmann, R. Sizing of the energy storage system of hybrid-electric aircraft in general aviation. *CEAS Aeronaut. J.* **2017**, *8*, 53–65. [CrossRef]
20. Riboldi, C.; Gualdoni, F. An integrated approach to the preliminary weight sizing of small electric aircraft. *Aerosp. Sci. Technol.* **2016**, *58*, 134–149. [CrossRef]
21. Hospodka, J.; Bínová, H.; Pleninger, S. Assessment of All-Electric General Aviation Aircraft. *Energies* **2020**, *13*, 6206. [CrossRef]
22. Salucci, F.; Trainelli, L.; Bruglieri, M.; Riboldi, C.E.; Rolando, A.L.; García González, G. Capturing the Demand for an Electric-Powered Short-Haul Air Transportation Network. In Proceedings of the AIAA SciTech Forum, Nashville, TN, USA, 11–15 January 2021. [CrossRef]
23. Orefice, F.; Marciello, V.; Nicolosi, F.; Zhang, Q.; Wortmann, G.; Menu, J.; Cusati, V. Design of Hybrid-Electric Small Air Transports. *IOP Conf. Ser. Mater. Sci. Eng.* **2022**, *1226*, 012075. [CrossRef]
24. Orefice, F.; Nicolosi, F.; Della Vecchia, P.; Ciliberti, D. Aircraft conceptual design of commuter aircraft including distributed electric propulsion. In Proceedings of the AIAA Aviation Forum, Virtual, 15–19 June 2020. [CrossRef]
25. Rolando, A.; Salucci, F.; Trainelli, L.; Riboldi, C.E.; Khan, Y.M. On the Design of an Electric-Powered Micro-Feeder Aircraft. In Proceedings of the 1st Aerospace Europe Conference (AEC), Bordeaux, France, 25–28 February 2020.
26. Isikveren, A.T.; Fefermann, Y.; Maury, C.; Level, C.; Zarati, K.; Salanne, J.-P.; Pornet, C.; Thoraval, B. Pre-design of a commuter transport utilising Voltaic-Joule/Brayton motive power systems. *Aeronaut. J.* **2018**, *122*, 205–237. [CrossRef]
27. Ciliberti, D.; Della Vecchia, P.; Memmolo, V.; Nicolosi, F.; Wortmann, G.; Ricci, F. The Enabling Technologies for a Quasi-Zero Emissions Commuter Aircraft. *Aerospace* **2022**, *9*, 319. [CrossRef]
28. Donateo, T.; Ficarella, A. A Methodology for the Comparative Analysis of Hybrid Electric and All-Electric Power Systems for Urban Air Mobility. *Energies* **2022**, *15*, 638. [CrossRef]
29. Bacchini, A.; Cestino, E. Electric VTOL Configurations Comparison. *Aerospace* **2019**, *6*, 26. [CrossRef]
30. Palaia, G.; Abu Salem, K.; Cipolla, V.; Binante, V.; Zanetti, D. A Conceptual Design Methodology for e-VTOL Aircraft for Urban Air Mobility. *Appl. Sci.* **2021**, *11*, 10815. [CrossRef]
31. Finger, D.F.; Götten, F.; Braun, C.; Bil, C. Initial sizing for a family of hybrid-electric VTOL general aviation aircraft. *Deutsche Ges. Luft-Raumfahrt* **2018**. [CrossRef]
32. Graver, B.; Zhang, K.; Rutherford, D. *CO_2 Emissions From Commercial Aviation*; ICCT, The International Council on Clean Transportation: Washington, DC, USA, 2018. Available online: https://theicct.org/publications/co2-emissions-commercial-aviation-2018 (accessed on 15 January 2023).

33. Pornet, C.; Gologan, C.; Vratny, P.C.; Seitz, A.; Schmitz, O.; Isikveren, A.T.; Hornung, M. Methodology for Sizing and Performance Assessment of Hybrid Energy Aircraft. *J. Aircr.* **2015**, *52*, 341–352. [CrossRef]
34. Pornet, C.; Isikveren, A. Conceptual design of hybrid-electric transport aircraft. *Prog. Aerosp. Sci.* **2015**, *79*, 114–135. [CrossRef]
35. Ang, A.W.X.; Rao, A.G.; Kanakis, T.; Lammen, W. Performance analysis of an electrically assisted propulsion system for a short-range civil aircraft. *Proc. Inst. Mech. Eng. Part G J. Aerosp. Eng.* **2018**, *233*, 1490–1502. [CrossRef]
36. Gnadt, A.R.; Speth, R.L.; Sabnis, J.S.; Barrett, S.R. Technical and environmental assessment of all-electric 180-passenger commercial aircraft. *Prog. Aerosp. Sci.* **2018**, *105*, 1–30. [CrossRef]
37. Sgueglia, A.; Schmollgruber, P.; Bartoli, N.; Benard, E.; Morlier, J.; Jasa, J.; Martins, J.R.R.A.; Hwang, J.T.; Gray, J.S. Multidisciplinary Design Optimization Framework with Coupled Derivative Computation for Hybrid Aircraft. *J. Aircr.* **2020**, *57*, 715–729. [CrossRef]
38. de Vries, R.; Brown, M.; Vos, R. Preliminary Sizing Method for Hybrid-Electric Distributed-Propulsion Aircraft. *J. Aircr.* **2019**, *56*, 2172–2188. [CrossRef]
39. Karpuk, S.; Elham, A. Influence of Novel Airframe Technologies on the Feasibility of Fully-Electric Regional Aviation. *Aerospace* **2021**, *8*, 163. [CrossRef]
40. Voskuijl, M.; van Bogaert, J.; Rao, A.G. Analysis and design of hybrid electric regional turboprop aircraft. *CEAS Aeronaut. J.* **2017**, *9*, 15–25. [CrossRef]
41. Finger, F.; Braun, C.; Bil, C. Comparative Assessment of Parallel-Hybrid-Electric Propulsion Systems for Four Different Aircraft. *J. Aircr.* **2020**, *57*, 843–853. [CrossRef]
42. Hoelzen, J.; Liu, Y.; Bensmann, B.; Winnefeld, C.; Elham, A.; Friedrichs, J.; Hanke-Rauschenbach, R. Conceptual Design of Operation Strategies for Hybrid Electric Aircraft. *Energies* **2018**, *11*, 217. [CrossRef]
43. Masson, P.J.; Brown, G.V.; Soban, D.S.; Luongo, C.A. HTS machines as enabling technology for all-electric airborne vehicles. *Supercond. Sci. Technol.* **2007**, *20*, 748–756. [CrossRef]
44. Ganev, E. Selecting the Best Electric Machines for Electrical Power-Generation Systems: High-performance solutions for aerospace More electric architectures. *IEEE Electrif. Mag.* **2014**, *2*, 13–22. [CrossRef]
45. Bugga, R.; Krause, C.; Smart, M.; West, W.; Brandon, E. Battery for electric aviation. In Proceedings of the NAATBatt Annual Meeting & Conference, Pasadena, CA, USA, 10–13 February 2020. Available online: https://trs.jpl.nasa.gov/handle/2014/52585 (accessed on 15 January 2023).
46. Adu-Gyamfi, B.A.; Good, C. Electric aviation: A review of concepts and enabling technologies. *Transp. Eng.* **2022**, *9*, 100134. [CrossRef]
47. Vratny, P.; Gologan, C.; Pornet, C.; Isikveren, A.; Hornung, M. Battery Pack Modeling Methods for Universally-Electric Aircraft. In Proceedings of the 4th CEAS Air & Space Conference, Linköping, Sweden, 17–19 September 2013.
48. Vegh, J.M.; MacDonald, T.; Wendorff, A.; Alonso, J.J. Sizing Methods for Aircraft of Variable Propulsion System Complexity. In Proceedings of the 55th AIAA Aerospace Sciences Meeting, Grapevine, TX, USA, 9–13 January 2017. [CrossRef]
49. Ugwueze, O.; Statheros, T.; Horri, N.; Innocente, M.; Bromfield, M. Investigation of a Mission-based Sizing Method for Electric VTOL Aircraft Preliminary Design. In Proceedings of the AIAA SciTech Forum, San Diego, CA, USA, 3–7 January 2022. [CrossRef]
50. Eisenhut, D.; Moebs, N.; Windels, E.; Bergmann, D.; Geiß, I.; Reis, R.; Strohmayer, A. Aircraft Requirements for Sustainable Regional Aviation. *Aerospace* **2021**, *8*, 61. [CrossRef]
51. Palaia, G.; Zanetti, D.; Abu Salem, K.; Cipolla, V.; Binante, V. THEA-CODE: A design tool for the conceptual design of hybrid-electric aircraft with conventional or unconventional airframe configurations. *Mech. Ind.* **2021**, *22*, 19. [CrossRef]
52. Palaia, G. Design and Performance Assessment Methodologies for Box-Wing Hybrid-Electric Aircraft from Urban to Regional Transport Applications. Ph.D. Thesis, University of Pisa, Pisa, Italy, 2022. to be published.
53. Drela, M.; Youngren, H. AVL 3.36 User Primer, Online Software Manual. 2017. Available online: https://perma.cc/R35R-W29F (accessed on 15 January 2023).
54. Raymer, P. *Aircraft Design: A Conceptual Approach*; AIAA Education Series; American Institute of Aeronautics and Astronautics, Inc.: Washington, DC, USA, 1992; ISBN 0-930403-51-7.
55. Mattingly, J.D.; Heiser, W.H.; Daley, D.H. *Aircraft Engine Design*, 3rd ed.; American Institute of Aeronautics and Astronautics: Washington, DC, USA, 2018. Available online: https://arc.aiaa.org/doi/book/10.2514/4.105173 (accessed on 15 January 2023).
56. Sforza, P.M. *Commercial Airplane Design Principles*, 1st ed.; Butterworth–Heinemann: Oxford, UK, 2014. Available online: https://www.sciencedirect.com/book/9780124199538/commercial-airplane-design-principles (accessed on 15 February 2023).
57. Federal Aviation Administration, FAR 25, Airworthiness Standards: Transport Category Airplanes, 1980.
58. Wells, D.P.; Horvath, B.L.; McCullers, L.A. The Flight Optimization System Weights Estimation Method. *NASA Tech. Rep.* **2017**. Available online: https://ntrs.nasa.gov/citations/20170005851 (accessed on 15 January 2023).
59. Cipolla, V.; Abu Salem, K.; Palaia, G.; Binante, V.; Zanetti, D. A DoE-based approach for the implementation of structural surrogate models in the early stage design of box-wing aircraft. *Aerosp. Sci. Technol.* **2021**, *117*, 106968. [CrossRef]
60. Dever, T.P.; Duffy, K.P.; Provenza, A.J.; Loyselle, P.L.; Choi, B.B.; Morrison, C.R.; Lowe, A.M. Assessment of Technologies for Noncryogenic Hybrid Electric Propulsion. *Rep. NASA* **2015**, TP-2015-216588.
61. Pornet, C.; Kaiser, S.; Gologan, C. Cost-based flight technique optimization for hybrid energy aircraft. *Aircr. Eng. Aerosp. Technol.* **2014**, *86*, 591–598. [CrossRef]
62. Casarosa, C. *Meccanica del Volo*; Pisa University Press: Pisa, Italy, 2013; ISBN 978-8867410163.

63. Garza, F.; Morelli, E. A Collection of Nonlinear Aircraft Simulations in MatLab. *Tech. Memo* **2003**. NASA/TM-2003-212145. Available online: https://ntrs.nasa.gov/citations/20030013626 (accessed on 15 January 2023).
64. Stevens, B.; Lewis, F.; Johnson, E. *Aircraft Control and Simulation: Dynamics, Controls Design, and Autonomous Systems*; John Wiley & Sons: Hoboken, NJ, USA, 2015; ISBN 978-1-118-87098-3.
65. Yu, Y.; Yao, H.; Liu, Y. Aircraft dynamics simulation using a novel physics-based learning method. *Aerosp. Sci. Technol.* **2019**, *87*, 254–264. [CrossRef]
66. Howe, R. An improved numerical integration method for flight simulation. In Proceedings of the AIAA Flight Simulation Technologies Conference and Exhibit, Boston, MA, USA, 14–16 August 1989. [CrossRef]
67. Torres, S. Evaluation of Numerical Methods for Aircraft Trajectory Computation. In Proceedings of the IEEE/AIAA 37th Digital Avionics Systems Conference (DASC), London, UK, 23–27 September 2018; pp. 1–10. [CrossRef]
68. De Marco, A.; Trifari, V.; Nicolosi, F.; Ruocco, M. A Simulation-Based Performance Analysis Tool for Aircraft Design Workflows. *Aerospace* **2020**, *7*, 155. [CrossRef]
69. Trifari, V.; Ruocco, M.; Cusati, V.; Nicolosi, F.; De Marco, A. Java framework for parametric aircraft design—Ground performance. *Aircr. Eng. Aerosp. Technol.* **2017**, *89*, 599–608. [CrossRef]
70. Nicolosi, F.; De Marco, A.; Attanasio, L.; Della Vecchia, P. Development of a Java-based framework for aircraft preliminary design and optimization. *J. Aerosp. Inf. Syst.* **2016**, *13*, 234–242. [CrossRef]
71. De Marco, A.; Cusati, V.; Trifari, V.; Ruocco, M.; Nicolosi, F.; Della Vecchia, P. A java toolchain of programs for aircraft design. In Proceedings of the 6th CEAS Conference, Bucharest, Romania, 16–20 October 2017. Available online: https://www.iris.unina.it/retrieve/handle/11588/696606/156026/CEAS2017_Paper_ID214.pdf (accessed on 15 February 2023).
72. De Marco, A.; Di Stasio, M.; Della Vecchia, P.; Trifari, V.; Nicolosi, F. Automatic modeling of aircraft external geometries for preliminary design workflows. *Aerosp. Sci. Technol.* **2020**, *98*, 105667. [CrossRef]
73. Abu Salem, K.; Palaia, G.; Bianchi, M.; Zanetti, D.; Cipolla, V.; Binante, V. Preliminary Take-Off Analysis and Simulation of PrandtlPlane Commercial Aircraft. *Aerotec. Missili Spaz.* **2020**, *99*, 203–216. [CrossRef]
74. de Wringer, S.; Varriale, C.; Oliviero, F. A Generalized Approach to Operational, Globally Optimal Aircraft Mission Performance Evaluation, with Application to Direct Lift Control. *Aerospace* **2020**, *7*, 134. [CrossRef]
75. Kim, D.; Seth, A.; Liem, R.P. Data-enhanced dynamic flight simulations for flight performance analysis. *Aerosp. Sci. Technol.* **2022**, *121*, 107357. [CrossRef]
76. Yanto, J.; Liem, R.P. Aircraft fuel burn performance study: A data-enhanced modeling approach. *Transp. Res. Part D Transp. Environ.* **2018**, *65*, 574–595. [CrossRef]
77. Schmollgruber, P. Enhancement of the Conceptual Aircraft Design Process through Certification Constraints Management and Full Mission Simulations. Ph.D. Thesis, Doctorat de l'Université de Toulouse délivré par l'Institut Supérieur de l'Aéronautique et de l'Espace, ISAE, Toulouse, France, 2018. Available online: https://hal.science/tel-02146110/ (accessed on 15 February 2023).
78. Schulz, S.; Ossmann, D.; Milz, D.; Kier, T.; Looye, G. Aircraft Mission Simulation Framework for Loads Analysis. In Proceedings of the AIAA Scitech Forum, Orlando, FL, USA, 6–10 January 2020. [CrossRef]
79. Gong, A.; Palmer, J.L.; Brian, G.; Harvey, J.R.; Verstraete, D. Performance of a hybrid, fuel-cell-based power system during simulated small unmanned aircraft missions. *Int. J. Hydrogen Energy* **2016**, *41*, 11418–11426. [CrossRef]
80. Liscouët-Hanke, S.; Pufe, S.; Maré, J.-C. A simulation framework for aircraft power management. *Proc. Inst. Mech. Eng. Part G J. Aerosp. Eng.* **2008**, *222*, 749–756. [CrossRef]
81. Liscouët-Hanke, S.; Maré, J.-C.; Pufe, S. Simulation framework for aircraft power system architecting. *J. Aircr.* **2009**, *46*, 1375–1380. [CrossRef]
82. Valdivia-Guerrero, V.; Foley, R.; Riverso, S.; Govindaraju, P.; Elsheikh, A.; Mangeruca, L.; Burgio, G.; Ferrari, A.; Gottschall, M.; Blochwitz, T.; et al. Modelling and Simulation Tools for Systems Integration on Aircraft. *SAE Tech. Pap.* **2016**. [CrossRef]
83. Abu Salem, K.; Giuseppe, P.; Vittorio, C.; Vincenzo, B.; Davide, Z.; Mario, C. Tools and methodologies for box-wing aircraft conceptual aerodynamic design and aeromechanic analysis. *Mech. Ind.* **2021**, *22*, 39. [CrossRef]
84. Hanlon, P. *Global Airlines. Competition in a Transnational Industry*, 3rd ed.; Routledge: New York, NY, USA, 2007. [CrossRef]
85. Husemann, M.; Schäfer, K.; Stumpf, E. Flexibility within flight operations as an evaluation criterion for preliminary aircraft design. *J. Air Transp. Manag.* **2018**, *71*, 201–214. [CrossRef]
86. Torenbeek, E. *Advanced Aircraft Design: Conceptual Design, Analysis and Optimization of Subsonic Civil Airplanes*; John Wiley & Sons: Hoboken, NJ, USA, 2013.